PERGAMON

Vacuum 68 (2003) 275–282

VACUUM
SURFACE ENGINEERING, SURFACE INSTRUMENTATION & VACUUM TECHNOLOGY

www.elsevier.com/locate/vacuum

Recent advances in ion-assisted growth of Cr/Sc multilayer X-ray mirrors for the water window

Jens Birch[a,*], Fredrik Eriksson[a], Göran A. Johansson[b], Hans. M. Hertz[b]

[a] *Thin Film Physics Division, IFM, Linköping University, SE-581 83 Linköping, Sweden*
[b] *Biomedical and X-ray Physics, Royal Institute of Technology, SCFAB, SE-106 91 Stockholm, Sweden*

Received 7 December 2001

Abstract

Cr/Sc multilayer X-ray mirrors intended for normal incidence reflection in the water window wavelength range, $\lambda = [2.4-4.4\,\text{nm}]$, have been grown by ion-assisted sputter deposition and characterized using soft and hard X-ray reflectivity. By extracting low-energy ions, with energies, E_{ion}, ranging from 9 to 113 eV and with ion-to-metal flux ratios, Φ , between 0.76 and 23.1, from the sputtering plasma to the growing film, the nano-structure of the multilayer interfaces could be modified. A significantly increased soft X-ray reflectivity, using $\lambda = 3.374\,\text{nm}$, for Cr/Sc multilayers with layer thicknesses in the range 0.4–2.8 nm, was obtained when high ion-to-metal flux ratios, $\Phi_{\text{Cr}} = 7.1$ and $\Phi_{\text{Sc}} = 23.1$, and low energy ions, $E_{\text{ion}} = 9\,\text{eV}$, were used. An experimental reflectivity of 5.5% was obtained at 76° for a multilayer with 400 bi-layers. Simulations of the reflectivity data showed that the interface widths are $<0.425\,\text{nm}$. It could be concluded that roughness of low spatial frequency is reduced at lower ion energies than the high spatial frequency which was eliminated at the expense of intermixing at the interfaces at higher ion energies. The predicted performance of normal incidence multilayer mirrors grown at optimum conditions and designed for $\lambda = 3.374$ and 3.115 nm indicates possible reflectivities of 6.5% and 14%, respectively.

Keywords: Multilayer; X-ray mirror; Water window; Chromium; Scandium; Ion-assisted growth; Sputtering

1. Introduction

Multilayer X-ray optics have many useful applications such as X-ray microscopy [1,2], X-ray astronomy [3,4], X-ray lithography [5], and X-ray microanalysis [6]. In particular, multilayer mirrors for X-rays with wavelengths, λ, in the water window region where $\lambda = [2.4-4.4\,\text{nm}]$, have an important application when used as optical elements in microscopy of biological specimens, due to the large absorption contrast between protein and water. In soft X-ray microscopy using a laser-plasma line source, which is our target application, a normal-incidence multilayer mirror is needed as a condenser to focus the X-rays on the specimen [7]. The performance of such mirrors is extremely sensitive to the multilayer design and the detailed structure of interfaces on a sub-nm scale which in turn are strongly influenced by the energetic species impinging on the surface during growth.

*Corresponding author. Tel.: +46-13-281228; fax: +46-13-137568.
E-mail address: jens.birch@ifm.liu.se (J. Birch).

0042-207X/03/$ - see front matter
PII: S0042-207X(02)00457-8

1.1. Multilayer design

The multilayer mirrors are built up by alternately depositing two materials, A and B, with different refractive indices to form a multilayer stack with an internal chemical modulation period, Λ, equal to the bi-layer thickness. Since the reflectance of a multilayer stack is the squared sum of the reflected amplitudes from each interface (neglecting absorption), a primary goal is to create the mirror with a certain Λ and a specific layer thickness ratio, optimized in order to give constructive interference. For normal incidence reflection of water window X-rays, this means that the individual layer thicknesses must be in the range 0.6–1.1 nm if the first-order interference maximum is to be utilized. The fraction of the amplitude reflected at each interface is given by the Fresnel reflection coefficient, r_{AB}:

$$|r_{AB}|^2 = \frac{(n_A - n_B)^2 + (k_A - k_B)^2}{(n_A + n_B)^2 + (k_A + k_B)^2}, \quad (1)$$

where $n_{A,B}$ and $k_{A,B}$ are the real and imaginary parts of the refractive indices, respectively, for the two materials. As n and k are strongly wavelength dependent and exhibit discontinuities at absorption edges in the X-ray spectrum, [8] Eq. (1) provides the main design rule when selecting materials for a particular wavelength. However, several complicating factors have to be considered. For example, a large difference in $k_{A,B}$ (the absorption coefficients) contributes to a large r_{AB} but it also means that the amplitude of the electromagnetic wave is attenuated very fast as it enters the multilayer such that only the interfaces close to the surface contributes to the total reflectivity which is thus reduced. Moreover, it must be possible to deposit the materials on top of each other with as flat and abrupt interfaces as possible. It can be shown that the normal incidence reflectivity, R, of a multilayer, to a first approximation, is influenced by the ratio between the interface width, σ, and the multilayer period, Λ, according to

$$R = R_0 e^{-(2\pi m(\sigma/\Lambda))^2}, \quad (2)$$

where R_0 is the theoretical reflectivity for an ideal structure ($\sigma = 0$) and m is the order of constructive interference [9]. As can be seen in Eq. (2), the absolute value of the interface width becomes more important at small multilayer periods [10,11]. Considering the different Λ required for different wavelengths, it is easy to realize why interface widths of $\sigma = 0.5$ nm may have a small effect on multilayer mirrors for extreme ultraviolet light (EUV) ($\Lambda \approx 5-50$ nm) while they will be absolutely devastating for water-window X-ray mirrors ($\Lambda \approx 1.2-2.2$ nm). The sensitivity in this wavelength range can be illustrated by a simple calculation using Eq. (2) which predicts that, for a semi-infinite Cr/Sc multilayer having a period $\Lambda = 1.692$ nm, designed for the wavelength $\lambda = 3.374$ nm, and a theoretical reflectivity $R_0 = 44\%$, an increase in interface width from 0.3 to 0.5 nm corresponds to a decrease in reflectivity from $R = 13\%$ to 1.4%. This explains why all reported experimental values of R in this wavelength range are very much lower than the ideal R_0 values. For example, for Cr/Sc $R_{0Cr/Sc} = 64\%$ while the best experimental value is $R_{Cr/Sc} = 11\%$ and for B_4C/W, $R_{0B4C/W} = 12\%$ while the best reported value is $R_{B4C/W} = 2.9\%$ [12]. This is also the reason why the vast majority of multilayer mirror research have aimed at applications using longer wavelengths.

The notion "interface width" contains two physically different aspects of an interface, the local chemical composition profile width (a result of atomic bulk displacement processes such as interdiffusion and intermixing), and interfacial roughness (related to surface displacement processes). Thus a rough interface may be uneven, yet locally abrupt, while an intermixed interface may be wide but still totally flat, as illustrated schematically in Fig. 1(a) and (c), respectively. Moreover, the schematic representation in Fig. 1(a) indicates that roughness can be separated into high and low spatial frequencies. The different interface features influence the reflectivity in a complex way and a detailed analysis requires computer simulations which in this work have been carried out using the IMD software [13].

1.2. Multilayer growth

Interface conditions are influenced by the deposition conditions in different ways. Interdiffusion is

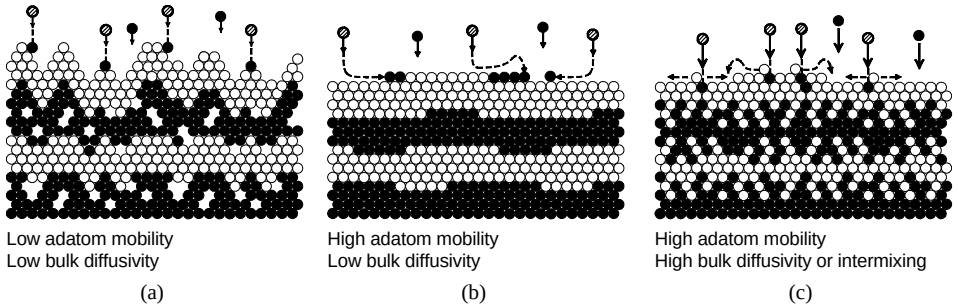

Fig. 1. A schematic view of different interfacial structures depending on relative mobilities at the surface and in the bulk of the multilayers. The cases shown are: (a) low adatom mobility and low bulk diffusivity, (b) high adatom mobility and low bulk diffusivity, and (c) both adatom mobility and bulk diffusivity are high or when intermixing occurs. Hatched atoms and broken lines show some trajectories of incoming (black) atoms, in (c) also surface diffusion of white atoms is indicated. The atomic structure is shown as close packed only for simplicity.

the thermally activated transport of material across the interface, and intermixing is related to the mixing of the interfaces due to energetic particle bombardment, while roughness usually is a consequence of limited adatom mobility on the growing surface. A low substrate temperature and no energetic particle irradiation during growth will minimize interdiffusion as well as intermixing. However, such conditions may lead to a kinetically limited growth with porous layers [14] and accumulating roughness as a consequence [15] as illustrated in Fig. 1(a). On the other hand, increasing the substrate temperature, in order to increase the adatom mobility and hence reduce accumulated roughness, may activate re-crystallization [16,17], thermal roughening [18] or bulk diffusion across the interfaces [19], as illustrated in Fig. 1(c). However, an optimal temperature, minimizing effects of both kinetically limited and thermally induced processes, has been found in the Mo/Si system [20]. These problems may be avoided by an apparent increase of the *surface* temperature, achieved by ion irradiation during growth, which will enhance adatom mobility while heating of the bulk multilayer is avoided, ideally leading to an interface structure as illustrated in Fig. 1(b). Such conditions, using >100 eV Ar ions, have been demonstrated to reduce the accumulated roughness and increased density of the layers, although on the expense of reduced interface abruptness due to intermixing of the interfaces in Si/Ge [21] and Mo/Si [22] amorphous multilayers. Many examples of negative effects of >100 eV ion irradiation during growth have been observed, such as resputtering and structural defect creation in Mo/V superlattices, [23] compressive stress evolution in Fe/Ni multilayers [24] as well as ion-incorporation and point defect generation in Mo [25]. One way to reduce the problem of intermixing is to ion-polish the surface after deposition of each layer in the multilayer by applying a grazing-incidence beam of 200–2000 eV ions from a separate Kauffman-type ion source [26].This technique has proven to significantly reduce roughnesses in Ni/C [27], W/C [28], Mo/Si [29], and Co/Cu [30] multilayers due to a combination of resputtering and viscous redistribution of atoms at the surface. However, post-deposition ion-polishing still allows the layers to grow under kinetic limitations leading to porous layers. Moreover, as the penetration depth of the ions, 0.5–5 nm [26,29], is of the same order as typical layer thicknesses in water window X-ray mirrors, intermixing of underlying interfaces cannot be avoided for this application. It is therefore desirable to reduce the ion energy to a level where bulk displacements are not induced but surface displacements still are stimulated, and to increase the ion flux to enhance adatom mobility. This should eliminate most of the negative interface effects while promoting the positive effects of ion-assisted growth. This approach has successfully been applied to epitaxial growth of several materials [31–33] where similar constraints

regarding the effects of ion-interface interactions have to be considered. Concurrent irradiation during growth, with 50 eV Ar ions from a separate source, has indeed shown to reduce long range lateral roughness without influencing the local structure of the interfaces in Ag/Fe multilayers [34] and a high flux of 24 eV N_2^+ ions have successfully been used to enable growth of CN_x/BN:C multilayers in a dual cathode sputtering discharge. A large variety of deposition techniques, including those using a separate ion source [35] and plasma-based deposition techniques [36], exists that might be used for ion-assisted deposition. In this article we report on recent advances in water window X-ray multilayer growth employing low-energy ion-assisted magnetron sputter deposition.

2. Experimental

All multilayer mirrors studied in this article have been grown in a dual-cathode magnetron sputter deposition system which has been described in detail elsewhere [23,37,38]. However, a few unique features of the system deserve to be mentioned as they are essential to the possibilities of low-energy ion-assisted growth. The circular magnetron sources have unbalanced type-II magnetic configurations with opposite polarities leading to strong magnetic fields from the outer poles extending into the chamber where they couple to each other or to a separate solenoid surrounding the substrate. During sputtering, secondary electrons from the cathodes are guided by the magnetic field to the substrate vicinity where they are allowed to ionize the sputtering gas. The ions are then attracted towards the substrate through a negative substrate bias voltage, V_S. In this way, a high flux of low-energy ions towards the growing film can be obtained. Ion-to-neutral flux ratios at the substrate ranging from 0.76 to 23.1 were achieved depending on the solenoid current used. The energy of the attracted ions was entirely determined by the difference between V_S and the plasma potential, V_P, since the mean free path for charge exchange collisions is about an order of magnitude longer than the sheath width for the sputtering pressure; 3 m Torr (0.4 Pa) and substrate bias voltages; 0–100 V, used in this work. The ion fluxes as well as V_P were determined through electrostatic plasma probe measurements [39]. Typical growth rates were 0.02–0.05 nm/s as determined by X-ray reflectivity thickness measurements.

The structural characterization of the multilayers was carried out by grazing incidence hard X-ray ($\lambda = 0.154$ nm) reflectivity (HXR) [40,41] and high resolution transmission electron microscopy in a Philips 20UT microscope. At-wavelength soft X-ray ($\lambda = 3.374$ nm) reflectivity (SXR) in the water-window was characterized using a reflectometer [42] based on the laser-plasma X-ray source being used also for X-ray microscopy [1,2]. The simulations of the HXR data were fitted using the WinGixa software [43] and the SXR simulations were performed using the IMD code [13].

3. Results and discussion

Cr/Sc is one of the best candidates for mirrors in the water window due to the Sc 2p absorption edge at 399 eV with large differences in n and k for X-ray energies just below the edge, hence giving large Fresnel coefficients (Eq. (2)). A high theoretical normal incidence reflectivity, $R_0 = 64\%$ (for a semi-infinite multilayer) right at the Sc edge, i.e., for $\lambda = 3.115$ nm, thus points at great potential for this material combination. Although, the reported experimental values are rather low, $R \leqslant 11\%$ [44–47], it should be noted that they still are the highest reported reflectivities for water window wavelengths. The mirrors in this work have been optimized for the C-VI emission line, $\lambda = 3.374$ nm, of a laser ethanol-plasma source used for X-ray microscopy, and the number of bilayers were limited to realistic values, $\leqslant 400$, which means that $R_0 \leqslant 35\%$.

Plasma probe measurements showed that the ion-to-metal flux ratios to the growing multilayer increased by a factor of 10, from $\Phi_{Cr} = 0.76$ and $\Phi_{Sc} = 2.5$ to $\Phi_{Cr} = 7.1$ and $\Phi_{Sc} = 23.1$, when the solenoid was used.

To illustrate the high structural order in the as-grown multilayers and the power of hard and soft X-ray reflectivity (HXR and SXR) analyses, a couple of examples are shown in Figs. 2 and 3. The

lower curve in Fig. 2 shows a typical HXR measurement of a mirror and the top curve is the corresponding simulation. The three major peaks ($n = 1$, 2 and 3) are the first three orders of multilayer Bragg reflections, and their positions at $2\theta_1 = 2.65^\circ$, $2\theta_2 = 5.22^\circ$ and $2\theta_3 = 7.79^\circ$ correspond to a multilayer period of $\Lambda = 3.410$ nm, as

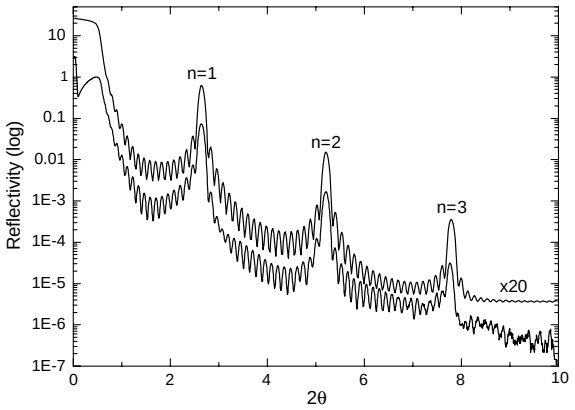

Fig. 2. Hard X-ray reflectivity measurement of a multilayer containing 20 bi-layers designed for the second-order normal reflection of $\lambda = 3.374$ nm, grown with an ion energy of 24 eV and ion-to-neutral flux ratios $\Phi_{Cr} = 7.1$ and $\Phi_{Sc} = 23.1$. The top curve shows the simulation, multiplied by a factor of 20 times for clarity.

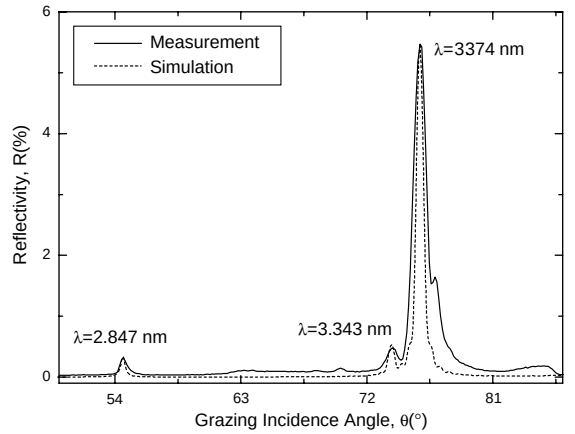

Fig. 3. Soft X-ray reflectivity measurement of a multilayer consisting of 400 bi-layers grown using high ion fluxes and an ion energy of 24 eV optimized for the first-order reflection of $\lambda = 3.374$ nm together with a simulation. Since the soft X-ray source has an ethanol target the spectrum contains several wavelengths which are also detected.

determined from the modified Bragg's law [48] by linear regression of $\sin^2\theta$ vs. n^2. In between each two neighboring Bragg peaks, 19 very distinct destructive interference fringes are visible due to the finite thickness of the multilayer being 20 times the period Λ. The regular appearance of these fringes is an evidence of a very high layer conformity. Above the critical angle, $2\theta_C = 0.53^\circ$, the simulation, which corresponds very well with the measurement, yielded individual layer thicknesses of $d_{Sc} = 2.766$ nm and $d_{Cr} = 0.641$ nm, i.e., a period of $\Lambda = 3.407$ nm. This is in very good agreement with calculation using the Bragg peak positions. The average interface width of the multilayer was determined to be 0.962 nm, and a CrO_x surface layer with a roughness of 1.32 nm was identified.

The solid line in Fig. 3 shows an at-wavelength ($\lambda = 3.374$ nm) soft X-ray reflectivity measurement obtained from a multilayer deposited with high ion fluxes and an ion energy of 24 eV. A peak reflectivity of $R = 5.5\%$ at a grazing incidence angle of 76° (peak labeled $\lambda = 3.374$ nm) was obtained for these conditions, which is quite high, considering that the X-ray wavelength is 0.25 nm above the Sc absorption edge. The small peaks labelled $\lambda = 2.847$ and 3.343 nm stem from parasitic wavelengths from the X-ray source. The dotted line shows the corresponding simulation, including all three wavelengths, assuming a period $\Lambda = 1.746$ nm and an average interface width $\sigma = 0.425$ nm.

To study the effects of different Ar-ion energies and fluxes, HXR as well as SXR were performed on a series of multilayers designed to have the second-order reflection $\lambda = 3.374$ nm at near-normal incidence. The multilayers, containing 20 bi-layers, were grown with different ion energies at low ($\Phi_{Cr} = 0.76$, $\Phi_{Sc} = 2.5$) and high ($\Phi_{Cr} = 7.1$, $\Phi_{Sc} = 23.1$) flux ratios. In Fig. 4 the peak intensities of the first three HXR Bragg reflections ($n = 1$, 2, and 3) are plotted as a function of the ion energy for the two flux situations. For the case of low Φ_{Cr} and Φ_{Sc}, the first peak increases for all ion energies while the second and third peaks, which are more roughness sensitive, decrease for energies above 73 eV, showing that an optimal ion energy exists for reducing the roughness, as seen

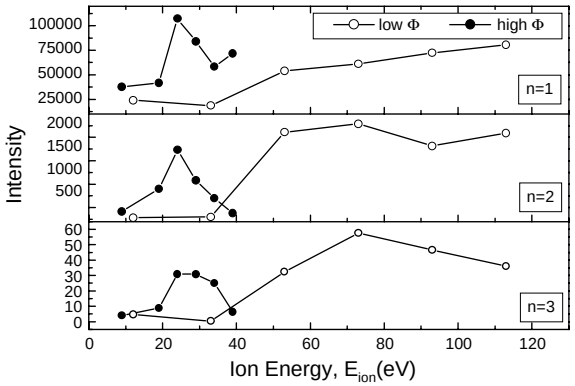

Fig. 4. Hard X-ray specular reflectivity of the first three orders (n) of multilayer Bragg reflections as a function of the ion energy for low and high ion fluxes, Φ.

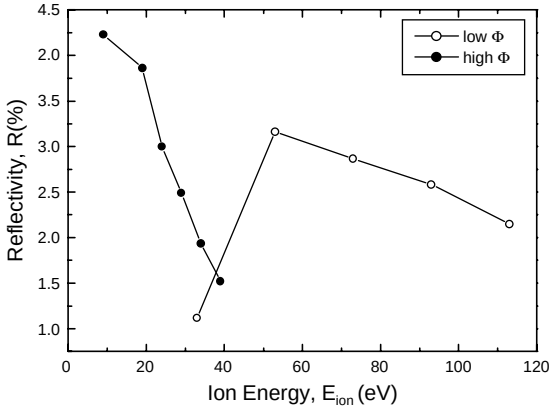

Fig. 5. Soft X-ray reflectivity of the first-order reflection of $\lambda = 3.374$ nm as a function of the ion energy for low and high ion fluxes, Φ.

by hard X-rays. For the multilayers deposited with large Φ_{Cr} and Φ_{Sc}, the optimum is shifted down to 24 eV ion energy. For ion energies below these optima, the increasing reflectivities with increasing energy are due to decreased interface roughnesses. This can be attributed to an increase in surface mobility, caused by the attracted Ar ions, during the whole deposition of each layer. An increase in surface mobility allows the deposited adatoms to move around on the surface and find positions with a local energy minimum, which in turn means a position that smoothens the surface. For a continuing increase in ion energy beyond the reflectivity maxima at 73 and 24 eV the observed decreases are due to the knock-on effects of the increasing energy of the Ar ion bombardment, resulting in intermixing of the layer materials. The same effects have been observed in amorphous Si/Ge [21] and Mo/Si [22] multilayers. Other possible explanations of decreased reflectivities at "high" ion energies may be roughening due to sputter erosion [49,50], ion-stimulated island formation [51], or thermal roughening [18,52,53]. However, the HXR Bragg peaks exhibited decreasing rocking curve widths for increasing ion energies, for both low and high fluxes, showing that the interlayer roughness correlation decreased, thus excluding increased roughness as the cause of decreased reflectivity.

Fig. 5 shows the first-order ($n = 1$) soft X-ray reflectivities, appearing at $\sim 30^\circ$ grazing incidence angle, of the same series of multilayers as shown in Fig. 4. Again the reflectivity shows a peak-shaped behavior for the case of low Ar^+ flux, but now with a maximum for an ion energy of about 53 eV. The reflectivity for the high Ar flux has its highest value for 9 eV ions, corresponding to growth with the sample at floating potential. The reason for these reflectivity behaviors follow the same arguments as given above for the hard X-ray reflectivities. The increase in reflectivity is due to the decreased roughness and then after a certain ion energy the intermixing takes over and the reflectivity decreases. Notable is the much higher maximal absolute reflectivity that occurs already for 9 eV ions using high flux conditions. A comparison of Figs. 4 and 5 reveals that soft X-ray reflectivity yields maximal reflectivities at approximately 20 eV lower energies than hard X-rays. Estimations of the X-ray coherence lengths for our experimental setups [54], in the directions parallel and perpendicular to the interfaces, here denoted $L_{//}$ and $L_{\perp}$, respectively, show that $L_{\perp}$ is in the order of 0.1 μm for both HXR and SXR while $L_{//}$ is in the order of 10 μm for SXR and only 0.025 μm for HXR. Thus we can conclude that low spatial frequency roughness, for which only SXR is sensitive, is reduced using lower ion energies than the high spatial frequency roughness which mainly affects HXR.

An estimation of the possible performance of normal incidence Cr/Sc mirrors, synthesized by

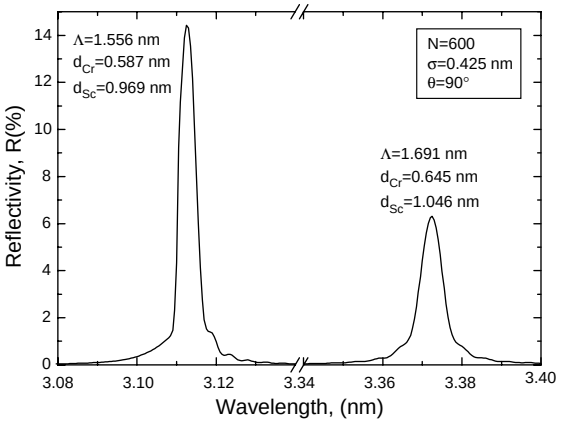

Fig. 6. Predicted normal incidence soft X-ray reflectivities of two mirrors designed for the X-ray wavelengths, $\lambda = 3.115$ and 3.374 nm, respectively. Both mirrors were modeled with 600 bi-layers and 0.425 nm interface widths.

ion-assisted sputtering, was made by performing simulations of the reflectivities from two multilayers, designed for $\lambda = 3.374$ and 3.115 nm, respectively, containing 600 bi-layers with interface widths equal to the determined 0.425 nm. The results are shown in Fig. 6 where it can be seen that possible reflectivities of 6.5% and 14% can be reached for the two wavelengths. Experiments to verify these numbers are being carried out and will be reported in a coming article.

4. Conclusions

Low-energy ion-assisted sputter deposition is beneficial in reducing the roughness in Sc/Cr multilayer X-ray mirrors grown at room temperature through stimulated adatom mobility. At very low energies, ($< \sim 25$ eV) and high enough ion-to-neutral flux ratios, Φ_{Cr} and Φ_{Sc} (~ 10 ions/atom) low spatial frequency roughening is reduced without any notable intermixing. The highest soft X-ray reflectivity at a grazing angle of $\sim 30^\circ$ was found when 9 eV ions were used. When low values of Φ are used (~ 1 ion/atom) rough interfaces are obtained unless ion energies higher than 50–70 eV are used. At these energies mainly high spatial frequency roughening is reduced, although at the expense of kinetic intermixing of the interfaces leading to a reduction of the reflectivity. A reflectivity of 5.47% at 76° for $\lambda = 3.374$ nm X-rays was obtained from a multilayer containing 400 bi-layers grown using 24 eV ions. Simulations of these reflectivity data gave interface widths of 0.425 nm. Using 24 eV ions, simulations showed that it is possible to obtain reflectivities of 6.5% and 14% for $\lambda = 3.374$ and 3.115 nm, respectively. However, as the reflectivity is about twice as high using 9 eV ions, there is room for further improvements in reflecting performance of normal incidence mirrors using this technique.

References

[1] Berglund M, Rymell L, Peuker M, Wilhein T, Hertz HM. J Microsc 2000;197:268–73.
[2] Hertz HM, Berglund M, Johansson GA, Peuker M, Wilhein T, Brismar H. In: Mayer-Ilse W, Warwick T, Attwood D, editors. X-ray microscopy. American Institute of Physics, 2000. pp. 721.
[3] Walker Jr. ABC, Barbee Jr. TW, Hoover RB, Lindblom JF. Science 1988;241:1781.
[4] Spiller E, Stearns DG, Krumrey M. Appl Phys 1993; 74:107–18.
[5] Stearns DG, Rosen RS, Vernon SP. Appl Opt 1993;32: 6952–60.
[6] Grudsky A, Rudnev A. Optics and microanalysis 1992. Proceedings of the 13th International Congress. Bristol, UK: IOP, 1993. p. 95–8.
[7] Hertz HM, Rymell L, Berglund M, Johansson GA, Wilhein T, Platonov Y, Broadway D. X-ray Optics, Instruments, and Missions II, SPIE Annual Meeting. Proc SPIE 1999;3766:247.
[8] Henke BL, Gullikson EM, Davis JC. At Data Nucl Data Tables 1993;54(2):181–342.
[9] Bennet HE, Bennet JM. Physics of thin films. New York: Academic Press, 1969.
[10] Walton CC, Thomas G, Kortright JB. Acta Mater 1998; 46:3767–75.
[11] Andreev SS, Müller SR, Platonov YuYa, Polushkin NI, Salashchenko NN, Schäfers F, Shinkarev SI, Simanovsky DM, Zuev SYu. Proc PIE "Superintense Laser Fields" 1991;1800:195–208.
[12] Wood J, Platonov Y. web-site: http://www-cxro.lbl.gov/multilayer/survey.html
[13] Windt DL. Comput Phys 1998;12:360–70.
[14] Hoedemaker M, van der Kuur J, Melker EJ, Thijsse BJ. Nucl Instrum Methods B 1997;127/128:888–92.
[15] Fullerton EE, Schuller IK, Bruynseraede Y. MRS Bull 1992;XVII(12):33.
[16] Ziegler E, Lepêtre Y, Schuller IK, Spiller E. Appl Phys Lett 1986;48:1354–6.

[17] Jankowski AF, Makowiecki DM, Wall MA, McKernan MA. J Appl Phys 1989;65:4450–1.
[18] Birch J, Hultman L, Sundgren J-E, Radnoczi G. Phys Rev B 1996;53:8114.
[19] Birch J, Yamamoto Y, Hultman L, Radnoczi G, Sundgren J-E, Wallenberg LR. Vacuum 1990;41:1231.
[20] Voorma H-J, Louis E, Koster NB, Bijkerk F. J Appl Phys 1998;83:4700–8.
[21] Järrendahl K, Birch J, Hultman L, Wallenberg LR, Radnoczi G, Arwin H, Sundgren J-E. Mater Res Soc Symp Proc 1992;258:571.
[22] Vernon SP, Stearns DG, Rosen RS. Appl Opt 1993: 6969–74.
[23] Håkansson G, Birch J, Hultman L, Ivanov IP, Sundgren J-E, Wallenberg LR. J Crys Growth 1992;121:399.
[24] Kim C, Qadri SB, Yu HY, Kim KH, Maruyama B, Edelstein AS. J Vac Sci Technol A 1990;8(3):1407–10.
[25] van der Linden JC, Seijbel LJ, Thijsse BJ. Nucl Instrum Methods B 1999;148:98–103.
[26] Puik EJ, van der Wiel MJ, Zeijlemaker H, Verhoeven J. Rev Sci Instrum 1992;63(1):1415–9.
[27] Puik EJ, van der Wiel MJ, Verhoeven J, Zeijlemaker H. Thin Solid Films 1990;193/194:782.
[28] Puik EJ, van der Wiel MJ, Zeijlemaker H, Verhoeven J. Appl Surf Sci 1991;47:63.
[29] Voorma H-J, Louis E, Bijkerk F, Abdali S. J Appl Phys 1997;82(4):1876–81.
[30] Pollard RJ, Wilson MJ, Grundy PJ. J Appl Phys 1994; 76(10):6090–2.
[31] Atwater HA. Solid State Phenom 1992;27:67–106.
[32] Tungasmita S, Birch J, Persson POÅ, Järrendahl K, Hultman L. Appl Phys Lett 2000;76:170.
[33] Gall D, Petrov I, Hellgren N, Hultman L, Sundgren J-E, Greene JE. J Appl Phys 1998;84(11):6034–41.
[34] Gladyszewski G, Jaouen C, Declemy A, Girard JC, Guerin P. Thin Solid Films 1998;319:44–8.
[35] Martin PJ. J Mater Sci 1986;21:1–25.
[36] Schneider JM, Rohde S, Sproul WD, Matthews A. J Appl D: Appl Phys 2000;33:173–86.
[37] Engström C, Berlind T, Birch J, Hultman L, Ivanov IP, Kirkpatrick SR, Rohde S. Vacuum 2000;56:107.
[38] Eriksson F, Johansson GA, Hertz HM, Birch J. Opt Engng 2002;41: in press.
[39] Petrov I, Orlinov V, Ivanov I, Kourtev J. Contrib Plasma Phys 1988;28(2):157–67.
[40] de Boer DKG. Phys Rev B 1991;44:498.
[41] Zabel H. Appl Phys A 1994;58:159–68.
[42] Johansson GA, Berglund M, Eriksson F, Birch J, Hertz HM. Rev Sci Instr 2001;72(1):58.
[43] WinGIXA simulation software by Philips Analytical, described in de Boer DKG, Leenaers AJG. Physica D 1996;221:18–26.
[44] Schäfers F, Mertin M, Abramsohn D, Gaupp A, Mertins H-Ch, Salashenko NN. Nucl Instrum Methods A 2001; 467–468:349–53.
[45] Salashchenko NN, Shamov EA. Opt Commun 1997;134: 7–9.
[46] Salashchenko NN, Fraerman AA, Mitenin SV, Prokhorov KA, Shamov EA. Nucl Instrum Methods A 1998;405: 292–6.
[47] Schäfers F, Mertins H-C, Schmolla F, Packe I, Salaschenko NN, Shamov EA. Appl Opt 1998;37(4):719.
[48] Agarvall BK. X-ray spectroscopy—an introduction. Berlin: Springer, 1979.
[49] Kahng B, Jeong H, Barabási A-L. Appl Phys Lett 2001; 78(6):805–7.
[50] Facsko S, Dekorsy T, Koerdt C, Trappe C, Kurz H, Vogt A, Hartnagel HL. Science 1999;285:1551.
[51] Hasan M-A, Knall J, Barnett SA, Rockett A, Sundgren J-E, Greene JE. J Vac Sci Technol A 1987; 5:1883–7.
[52] Bennema P. J Phys D 1993;26:B1.
[53] Weeks JD, Gilmer GH. In: Prigogine I, Rice SA, editors. Advances in chemistry and physics. New York: Wiley, 1979. p. 157.
[54] Als-Nielsen J, McMorrow D. Elements of modern X-ray physics. Chichester: Wiley, 2001.